Sediment pulses in mountain rivers: 2. Comparison between experiments and numerical predictions

Yantao Cui[1] and Gary Parker
St. Anthony Falls Laboratory, University of Minnesota, Minneapolis, Minnesota, USA

James Pizzuto
Department of Geology, University of Delaware, Newark, Delaware, USA

Thomas E. Lisle
Pacific Southwest Research Station, Forest Service, U. S. Department of Agriculture, Arcata, California, USA

Received 28 October 2002; revised 21 April 2003; accepted 18 June 2003; published 10 September 2003.

[1] Mountain rivers in particular are prone to sediment input in the form of pulses rather than a more continuous supply. These pulses often enter in the form of landslides from adjacent hillslopes or debris flows from steeper tributaries. The activities of humans such as timber harvesting, road building, and urban development can increase the frequency of sediment pulses. The question as to how mountain rivers accommodate pulses of sediment thus becomes of practical as well as academic significance. In part 1 [*Cui et al.*, 2003], the results of three laboratory experiments on sediment pulses are reported. It was found there that the pulses were eliminated from the flume predominantly by dispersion of the topographic high. Significant translation was observed only when the pulse material was substantially finer than the ambient load in the river. Here the laboratory data are used to test a numerical model originally devised for predicting the evolution of sediment pulses in field-scale gravel bed streams. The model successfully reproduces the predominantly dispersive deformation of the experimental pulses. Rates of dispersion are generally underestimated, largely because bed load transport rates are underestimated by the transport equation used in the model. The model reproduces the experimental data best when the pulse is significantly coarser than the ambient sediment. In this case, the model successfully predicts the formation and downstream progradation of a delta that formed in the backwater zone of the pulse in run 3. The performance of the model is less successful when the pulse is composed primarily of sand. This is likely because the bed load equation used in the study is specifically designed for gravel. When the model is adapted to conditions characteristic of large, sand bed rivers with low Froude numbers, it predicts substantial translation of pulses as well as dispersion. *INDEX TERMS:* 1803 Hydrology: Anthropogenic effects; 1815 Hydrology: Erosion and sedimentation; 1824 Hydrology: Geomorphology (1625); 3210 Mathematical Geophysics: Modeling; *KEYWORDS:* sediment transport, sediment pulses, sediment waves, mountain rivers, numerical simulation

Citation: Cui, Y., G. Parker, J. Pizzuto, T. E. Lisle, Sediment pulses in mountain rivers: 2. Comparison between experiments and numerical predictions, *Water Resour. Res.*, *39*(9), 1240, doi:10.1029/2002WR001805, 2003.

1. Introduction

[2] A sediment pulse is a discrete input of a significant amount of sediment into a river that results in a transient topographic high on the bed. Sediment pulses are particularly characteristic of mountain streams, where they are associated with landslides from adjacent hillslopes or debris flows from steeper tributaries. In extreme cases, a pulse can completely block the flow of the river for a time, creating a natural dam that is eventually breached by overflow from the reservoir that forms behind it [*Li et al.*, 1986].

[3] A central question concerning sediment pulses is how the river responds to and deforms them. The transient topographic high may be translated downstream as a sediment wave [*Benda and Dunne*, 1997], dispersed in place [*Lisle et al.*, 1997] or undergo some combination of these deformations. In addition, if the material in the pulse is sufficiently weak, a significant amount may be abraded into silt or sand.

[4] The question of translation versus dispersion was addressed via laboratory experiments in part 1 [*Cui et al.*, 2003]. The small scale of the experiments and durability of the sediment used in them allowed the neglect of abrasion. A complete description of the experiments is given in part 1. Only a few relevant points are mentioned here. The channel was 0.5 m wide and 45 m long with vertical, inerodible

[1]Now at Stillwater Sciences, Berkeley, California, USA.

0043-1397/03/2002WR001805$09.00

sidewalls. An ambient mobile-bed equilibrium was created by feeding in a sediment mix that was half gravel and half sand, so that the median feed size D_{f50} was 2 mm and the maximum size was 8 mm. This ambient equilibrium, which had a surface geometric mean grain size of 3.14–3.43 mm, subsurface geometric mean grain size of 2.58–2.85 mm, a flow depth h of 0.0325 m, a bed slope S of 0.0108 and a Froude number *Fr* of 0.98, was used as the base state for all experiments on pulses. The dominant mode of sediment transport was bed load, although some of the finer sand was observed to be in suspension. The mobile bed so created was mildly armored.

[5] Results for experiments with three types of pulses are reported in part 1; a case for which the pulse material was the same as that of the ambient sediment feed, a case for which it was significantly coarser, and a case for which it was significantly finer. The dominant mode of pulse elimination was dispersion in all cases. Only when the pulse sediment was significantly finer than the feed sediment was significant translation observed as well.

[6] *Cui and Parker* [2003] present a numerical model for the deformation of sediment pulses in mountain rivers that is specifically designed for field application. It has been used without calibration to successfully predict the fate of the sediment pulse created by a landslide into the Navarro River, California, in March 1995 [*Sutherland et al.*, 1998; *Hansler et al.*, 1998]. Here the model is tested against the experimental results of part 1.

[7] It should be noted from the outset that the model of *Cui and Parker* [2003] was designed to be used at field scale. The formulation used for sediment transport is that of *Parker* [1990a, 1990b], which is based solely on field data pertaining to gravel moving as bed load. The formulation is likely to lose some accuracy when applied to material no larger than pea gravel, and lose even more accuracy when applied to sand. This notwithstanding, a direct application of the model to the experimental data is given here. In the present analysis two parameters (reference Shields stress and ratio of roughness height to the thickness of the active layer) have been modestly adjusted so as to correctly simulate the ambient equilibrium mobile-bed conditions prevailing in the absence of a sediment pulse. No further adjustments have been made to the analysis.

[8] One may inquire as to why the experimental data were not compared with a sediment transport formulation that is more appropriate to the grain size distributions used in the experiment. There are two reasons why this was not done. The first of these is that the appropriate formulation did not yet exist at the time this model was developed. Such a formulation would have to provide simultaneous predictions of both gravel and sand transport on a grain size specific basis. Recently, *Wilcock and Crowe* [2003] have developed such an equation, which can be incorporated into the model in the future. The second of these is the desire to modify the model as minimally as possible from what might be expected to be applicable to the field.

2. Overview of the Numerical Model

[9] The numerical model is that of *Cui and Parker* [2003], but here simplified to the case of constant channel width, water discharge and sediment feed rate; vanishing (zero) water and sediment input from the banks; and vanishing abrasion. The approach is closely related to that described by *Cui et al.* [1996] and *Cui and Parker* [1997a]. Here a brief summary is given.

[10] The flow is described by the generalized 1-D St. Venant shallow water equations for water mass and momentum conservation;

$$\frac{\partial h}{\partial t} + \frac{\partial uh}{\partial x} = 0 \tag{1}$$

$$\frac{\partial u}{\partial t} + \frac{\partial}{\partial x}\left(\frac{1}{2}u^2 + gh + g\eta\right) + \frac{u_*^2}{h} = 0 \tag{2}$$

where x denotes down-channel distance, t denotes time, u denotes flow velocity; h denotes water depth; η denotes bed height, g denotes the acceleration of gravity and u_* denotes bed shear velocity.

[11] Sediment balance is based on a three-layer model; i.e., a bed load layer, a bed surface layer (active or exchange layer) of thickness L_a and a substrate layer. The complete development of the 1-D Exner equation of sediment balance for this model is given in *Parker* [1991a, 1991b]. Some modifications due to the work of *Cui et al.* [1996] have been incorporated in the formulation. Here it is useful to decompose the relation into one governing the evolution of bed elevation and the other for evolution of the grain size distribution of the surface layer. These take the following forms;

$$(1-\lambda_p)\frac{\partial \eta}{\partial t} + \frac{\partial q_G}{\partial x} = 0 \tag{3}$$

$$(1-\lambda_p)\left(\frac{\partial (L_a F_j)}{\partial t} + f_{I,j}\frac{\partial(\eta - L_a)}{\partial t}\right) + \frac{\partial\left(q_G p_j\right)}{\partial x} = 0 \tag{4}$$

In the above relations, the index j denotes the jth grain size range. Thus F_j denotes the fraction content by mass of the gravel in the jth grain size range in the surface layer. In addition, p_j denotes the same fraction content in the bed load, q_G denotes the total volume gravel transport rate per unit width summed over all size ranges and λ_p is a bed porosity. The parameter $f_{I,j}$ denotes the fraction content in the jth grain size range that is exchanged at the interface between the surface and substrate as the bed aggrades or degrades.

[12] Here grain sizes are characterized on the logarithmic Ψ scale, where Ψ is related to grain size D in mm and the more familiar ϕ scale by the relations

$$\psi = -\phi = \ell og_2(D) \tag{5}$$

Thus, if the jth grain size range is taken to be bounded by sizes D_j (Ψ_j) and D_{j+1} (Ψ_{j+1}), the mean size of this range $\overline{D_j}(\overline{\Psi})$ is given by

$$\overline{\Psi_j} = \left(\psi_j + \psi_{j+1}\right)/2 \tag{6a}$$

$$\overline{D_j} = 2^{\overline{\Psi_j}} = \sqrt{D_j D_{j+1}} \tag{6b}$$

The formulation of active layer thickness used here is based on that of *Cui et al.* [1996], which differs somewhat from *Parker* [1991a, 1991b]. It takes the form

$$L_a = D_{sg}\sigma_{sg}^{1.28} \tag{7}$$

where D_{sg} denotes the geometric mean size of the sediment in the surface layer and σ_{sg} denotes the geometric standard deviation of the sediment in the surface layer. The interfacial grain size fractions are given in accordance with the experimental results of *Toro-Escobar et al.* [1996];

$$f_{I,j} = \begin{cases} \chi p_j + (1-\chi)F_j\,, & \dfrac{\partial\eta}{\partial t} > 0 \\ p_{Sj}\,, & \dfrac{\partial\eta}{\partial t} < 0 \end{cases} \tag{8}$$

where $p_{S,j}$ denotes the fraction content in the jth size range of the substrate immediately below the active layer and the coefficient χ takes a value of 0.7.

[13] The gravel transport relation used here is that of *Parker* [1990a, 1990b]. The reader is referred to the original reference for details. It suffices to note that it calculates the magnitude and grain size distribution of the gravel load based on the size distribution of the surface layer and the boundary shear stress. It is based solely on field data for gravel. It was not intended for application to sand, or for material of any size moving in suspension. It thus imposes a lower bound of 2 mm in application. This bound cannot be preserved in the analysis reported here because half of the ambient feed sediment in the experiments of part 1 was sand. The lower bound used here has been reduced to 0.5 mm, without any modification to the gravel transport relation itself. This value is slightly larger than the grain size 0.41 mm at which the ratio of particle fall velocity to ambient shear velocity takes the value unity. It is thus larger than the coarsest grain size for which particle suspension might be inferred to be important. This notwithstanding, a degradation of the predictability of a relation can be expected when it is applied beyond its intended bounds. This is necessitated here because of the difficulty of performing experiments on gravel bed rivers at full field scale.

[14] In the experiments described in part 1, an ambient mobile-bed equilibrium was first established, and then a pulse of sediment was placed over this bed. The grain size distributions of both the sediment feed associated with the mobile-bed equilibrium and the sediment pulses are given in Figure 3 of part 1. It can be seen from Figure 3 of part 1 that 87% of the feed sediment was coarser than the lower bound of 0.5 mm used in the transport calculation. In the case of the finest pulse studied, 67% of the sediment was coarser than 0.5 mm.

[15] The model for bed resistance is the Keulegan-type formulation given by *Cui et al.* [1996];

$$\frac{u}{u_*} = 2.5\ell n\left(11\frac{h}{k_s}\right) \tag{9}$$

where roughness height k_s is given by the relation

$$k_s = \alpha L_a \tag{10}$$

[16] Two parameters were adjusted from the original *Parker* [1990a, 1990b] formulation in order to match the Froude number and bed slope at the ambient mobile-bed equilibrium in the absence of sediment pulses. The reference Shields stress τ^*_{rsgo} was adjusted from the original value of 0.0386 to 0.041, which is a 6% increase. The parameter α was adjusted from the original value of 2 to a value of 0.9, which is a 55% decrease. Both adjustments are quite modest, the latter one due to the logarithmic dependence of u/u_* on k_s. This adjustment was motivated by the need to ensure that the differences between computed and observed pulse evolution do not simply reflect differences in the ambient prepulse base state.

[17] The adjusted model is applied under a reference condition under which no sediment pulse is introduced. The result is a constant channel bed without aggradation and degradation.

3. Numerical Solution

[18] Details concerning the numerical solution of the relations for flow and sediment transport as used in field implementation are given by *Cui and Parker* [2003]. In that analysis, the quasi-steady approximation, according to which the terms in (1) and (2) containing time derivatives are neglected, is employed. These relations thus simplify to

$$uh = q_w \tag{11}$$

$$\left(1 - Fr^2\right)\frac{dh}{dx} = -\frac{\partial\eta}{\partial x} - \frac{u_*^2}{gh} \tag{12}$$

where q_w denotes the water discharge per unit width and *Fr* denotes the local Froude number of the flow.

[19] When the Froude number is sufficiently high and the sediment pulse sufficiently long the flow can be approximated as a quasi-steady flow obeying a quasi-normal momentum balance, according to which (12) further simplifies to

$$gh\frac{\partial\eta}{\partial x} + u_*^2 = 0 \tag{13}$$

[*Cui and Parker*, 1997a, 1997b]. Here the quasi-normal approximation is used wherever the Froude number exceeds 0.75; otherwise a stepwise backwater calculation is automatically performed on the full steady St. Venant equations. In light of the high Froude number of the ambient flow (0.98), the quasi-normal assumption was used through much of the solution domain as the pulse evolved. Each experimental pulse did create transient backwater behind it, however, requiring the use of the full backwater formulation in at least part of the domain. The above technique is thus sufficient to capture the interaction between the flow profile, the pulse and the bed as they coevolve.

[20] The initial condition for the simulation of bed evolution is the bed topography corresponding to the sediment pulse as emplaced. The measured antecedent bed was, however, smoothed to remove both random irregularities and those associated with alternate bars for use in the numerical model. In the numerical model, the measured initial pulse thickness profile was placed on top of this smoothed antecedent bed. The grain size distributions of the feed sediment, as well as those of the initial pulses used in

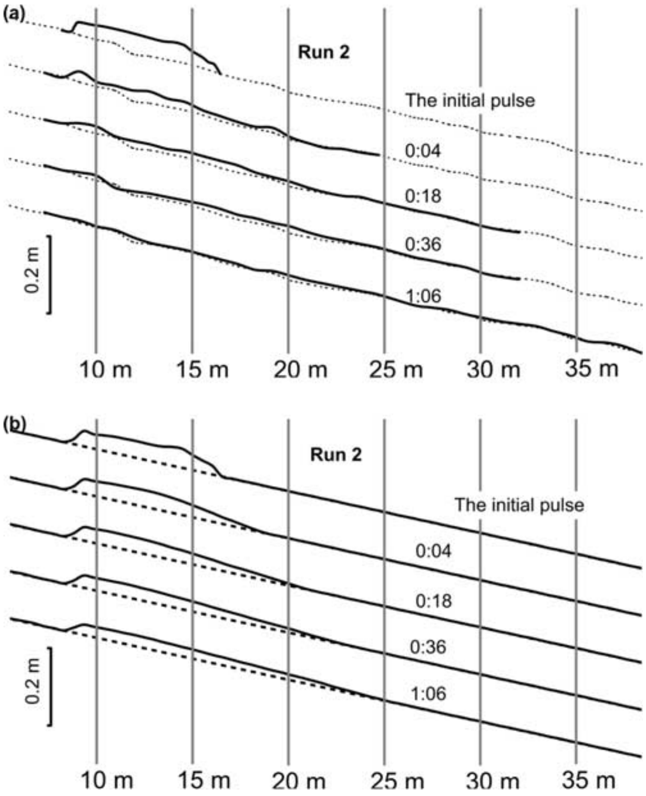

Figure 1. (a) Observed long profiles of cross-sectionally averaged bed elevation for run 2. The times are in (hour:min). (b) Simulated long profiles of bed elevation for run 2. The times are in (hour:min). Note that in the simulation the initial bed over which the pulse was placed has been smoothed. The profile of initial pulse thickness for the numerical run was identical to that of the experimental run; the profile of initial pulse top elevation differs slightly between the two only because of smoothing of the bed. These comments also apply to Figures 5 and 10.

the numerical model are the measured curves given in Figure 3 of part 1. The initial pulse is assumed to be completely unarmored. The downstream boundary condition consists of imposed normal flow with a fixed bed elevation.

4. Comparison With the Experimental Data

4.1. Run 2

[21] In this run, the pulse was composed of nearly the same material as the sediment feed, i.e., half sand and half pea gravel. The ratio D_{p50}/D_{f50} of pulse median size to feed median size was 1.1. The geometric mean grain size of the pulse sediment was 1.83 mm, finer than the prepulse surface and subsurface which had geometric mean grain sizes of 3.14 mm and 2.85 mm, respectively. The sediment feed had a median size D_{f50} of 2 mm in all runs. The pulse was placed over a length of 7.5 m starting 8 m from the point of sediment feed. The average height of the pulse was 3.5 cm. The material was completely unarmored as placed.

[22] The observed long profile of cross-sectionally averaged bed elevation is given in Figure 1a for the pulse as placed over the bed, and for the times 0:04, 0:18, 0:36 and 1:06, where the number to the left of the colon is hours and the number to the right is minutes. The corresponding numerical results are shown in Figure 1b. Both the observed and computed profiles show that dispersion dominated translation. The overall patterns are in reasonable agreement, but the numerical pulse deformed more slowly than the experimental one.

[23] The observed and predicted spatial variations in sediment transport rates are plotted for the times 0:05, 0:27, 1:17, 1:46 and 8:14 in Figures 2a and 2b, respectively. While there is considerable scatter in the experimental data, the model provides a generally faithful representation of the initial marked decrease in sediment transport load immediately upstream of the pulse and increase in sediment load downstream of the pulse, and then subsequent recovery with time toward ambient values. This effect gradually propagates downstream in time, becoming less pronounced as it does so. The rates of downstream propagation of the point of peak sediment transport rate predicted by the model are lower than the observed values. Note that the model predicts extremely low sediment transport rates over the upstream part of the pulse, a trend that is in general agreement with the data.

[24] Figure 3 shows the spatial and temporal variation in experimental and simulated arithmetic mean grain size in the substrate, as measured on the Ψ scale. Both the experimental and numerical results show a mild decline in

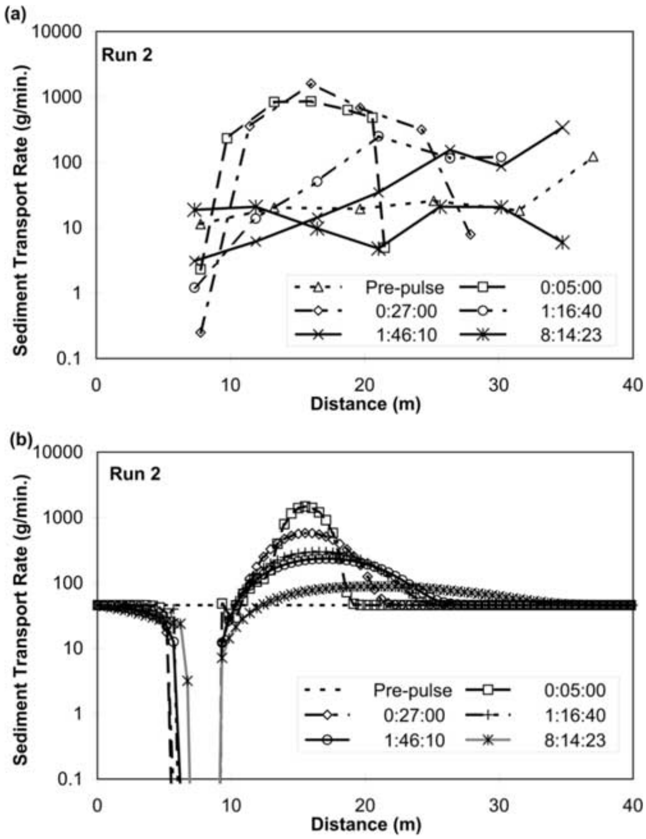

Figure 2. (a) Observed temporal and spatial variation in sediment transport rate for run 2. The times are in (hour:min). (b) Simulated temporal and spatial variation in sediment transport rate for run 2. The times are in (hour:min).

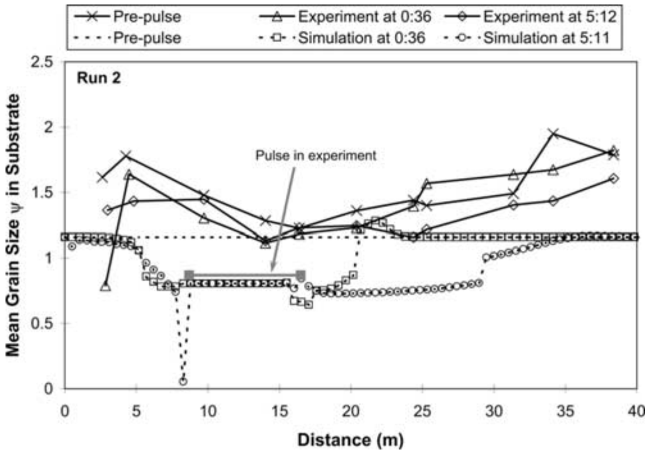

Figure 3. Simulated and observed temporal and spatial variation in substrate mean grain size on the ψ scale for run 2. The times are in (hour:min).

substrate mean grain size just downstream of the initial pulse, with a recovery farther downstream. The observed decline is, however, very slight and probably within the error of the measurements. The predicted values are low by a factor of about 0.4 Ψ units. Possible cause for this under-prediction includes errors in sampling data and the accuracy of equation (8), and a lower value for χ would have produced better results. The predicted curves show localized spikes near the beginning and end of the initial pulse that may be the artifacts of the calculation technique. It should be noted, however, that there is a physical reason that sediment deposit upstream of the pulse should be finer, i.e., the backwater from the pulse reduces coarse sediment transport to the area and promotes fine sediment deposition. In addition, the predicted curves also show a point downstream of which grain size rather abruptly increases toward the simulated prepulse value (with some overshoot). In the model this represents the downstream end of the propagating pulse. The experimental pulse did not have such a well-defined downstream end.

[25] The pulse shapes in Figure 1 can be used to compute moments yielding the coordinates of the centroid (x_c, y_c) of the pulse and the standard deviations (σ_x, σ_y) about the centroid in the following way;

$$(x_c, y_c) = \frac{\iint (x, y)dA}{\iint dA} \tag{14a}$$

$$\left(\sigma_x^2, \sigma_y^2\right) = \frac{\iint \left[(x - x_c)^2, (y - y_c)^2\right] dA}{\iint dA} \tag{14b}$$

Here the x coordinate is measured streamwise from the point of sediment feed and the y coordinate is measured upward from the ambient bed and dA denotes a differential area in the x-y plane. The predicted and measured values of x_c and $x_c \pm \sigma_x$ are given in Figure 4a. The numerical model notably under-predicts x_c, indicating a slower rate of elongation of the pulse as it dispersed. The spread of the pulse $x_c \pm \sigma_x$ was also consistently under-predicted. This is likely associated at least partially with an expected inability of the model to represent the measured fluctuations in the long profile of the pulses in Figure 1a. The cross-sectional average of the measured section elevation includes 2-D effects, for example, that cannot be reproduced in a 1-D model. Figure 4b shows the measured and predicted values of y_c and $y_c \pm \sigma_y$. The model overpredicted y_c, i.e., the average thickness of the patch, for the same reason that x_c was drastically under-predicted.

4.2. Run 3

[26] In this run the pulse was significantly coarser than the feed material, with a ratio D_{p50}/D_{f50} of 1.9. The geometric mean grain size of the pulse sediment was 3.05 mm, which is slightly finer than the prepulse surface geometric mean grain size of 3.43 mm and coarser than the prepulse substrate geometric mean grain size of 2.58 mm. The pulse was placed over a length of 7.5 m starting 8 m from the point of sediment feed. The average height of the pulse was 3.5 cm. The material was completely unarmored as placed.

[27] The observed and predicted long profiles are given in Figures 5a and 5b, respectively. The agreement is excellent. As a matter of fact, the agreement in long profile is even better than shown in Figures 5a and 5b. This is because the initial long profile measurements were conducted in detail,

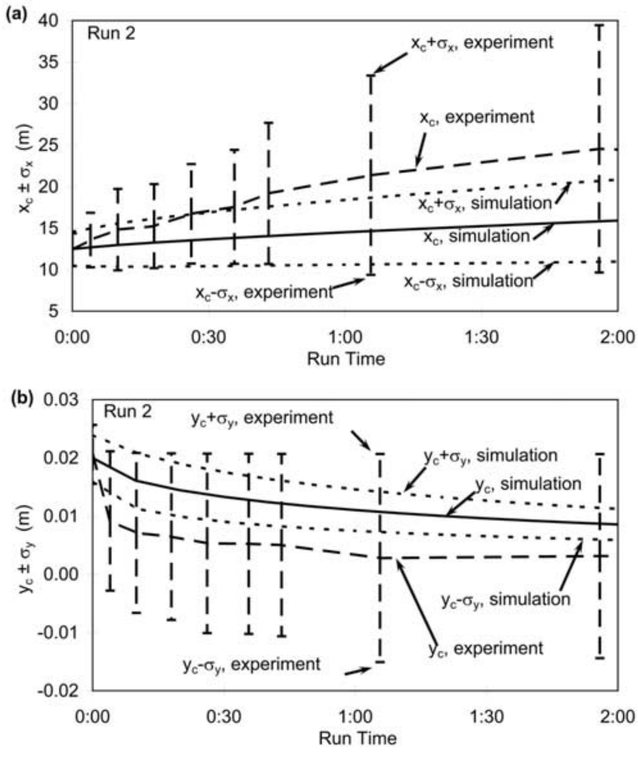

Figure 4. (a) Simulated and observed temporal variation in x_c and $x_c \pm \sigma_x$ for run 2. The vertical lines show the experimental spread from $x_c - \sigma_x$ to $x_c + \sigma_x$. (b) Simulated and observed temporal variation in y_c and $y_c \pm \sigma_y$ for run 2. The vertical lines show the experimental spread from $y_c - \sigma_y$ to $y_c + \sigma_y$.

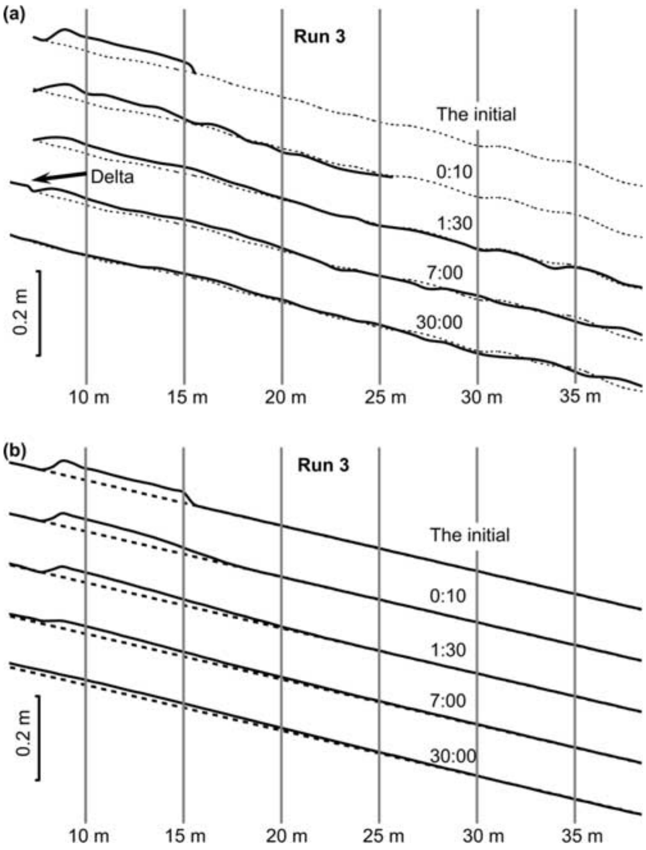

Figure 5. (a) Observed long profiles of cross-sectionally averaged bed elevation for run 3. The times are in (hour:min). (b) Simulated long profiles of bed elevation for run 3. The times are in (hour:min).

but the subsequent measurements were conducted at limited stations (see *Cui et al.* [2003] for details). This measurement technique caused the upper portion of the pulse appear to be deforming during the early stage of the experiment, while visual observations indicated that it evolved more slowly, as predicted in Figure 5b. The data for sediment transport rates in Figure 6a are sparse; all that can be said about the comparison with the computed values in Figure 6b is that the two are of the same order of magnitude. It should be noted, however, sediment transport rate for the experiment and the simulation both decline over time to similar values. Again note that the predicted and observed sediment transport rates in the backwater zone of the pulse that are so low that they plot off the scale shown in the figures. The observed values of mean grain size of Figure 7a are moderately well represented in the model, except for the fact that the observations did not show some detailed patterns appearing in the simulation. The lack of details in the experimental data may have been caused by the relatively small sampling volume in surface and subsurface samples. The agreement between the observed and predicted values of x_c and $x_c \pm \sigma_x$ in Figure 8a and y_c and $y_c \pm \sigma_y$ in Figure 8b is again much better than for run 2. The main discrepancy is a very rapid initial elongation observed in the very early stages of the experimental run, which may be associated with the observation technique used in the experiment, as discussed earlier.

[28] Figure 9 shows the predicted evolution of incremental bed elevation of the pulse above the ambient bed at a scale that allows the observation of detail. Note in particular the formation of a small delta just upstream of the pulse. This delta, which was created in response to the tendency for the pulse to dam the flow for a period, was also observed in the experiment. The model predicts that the delta should merge with the pulse, ultimately leading to upstream as well as downstream dispersion of the pulse. This behavior was observed not only in run 3 (see Figure 11 of part 1), but also in the case of the sediment pulse observed in the Navarro River, California [*Sutherland et al.*, 1998; *Hansler et al.*, 1998; *Lisle et al.*, 2001; *Sutherland et al.*, 2002]. It should be clearly noted that upstream dispersion of pulse elevation does not imply or require that any sediment move upstream.

4.3. Run 4b

[29] In this run the pulse was significantly finer than the feed material, the prepulse surface, and the prepulse substrate, with a ratio D_{p50}/D_{f50} of 0.31. The pulse was placed over a length of 7.4 m starting 6.8 m from the point of sediment feed. The average pulse height was 3.5 m. The material was completely unarmored when placed.

[30] The observed and predicted long profiles are given in Figures 10a and 10b, respectively. The leading and trailing edges of the pulse shown in Figure 10a were clearly observed during the experiment (sand over gravel). In the case of Figure 10b the positions of these edges were inferred

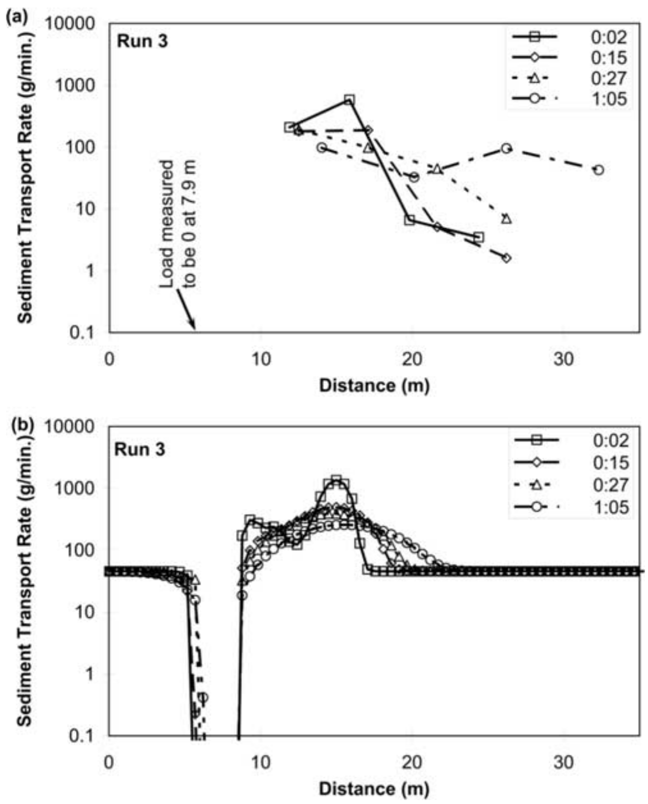

Figure 6. (a) Observed temporal and spatial variation in sediment transport rate for run 3. The times are in (hour:min). (b) Simulated temporal and spatial variation in sediment transport rate for run 3. The times are in (hour:min).

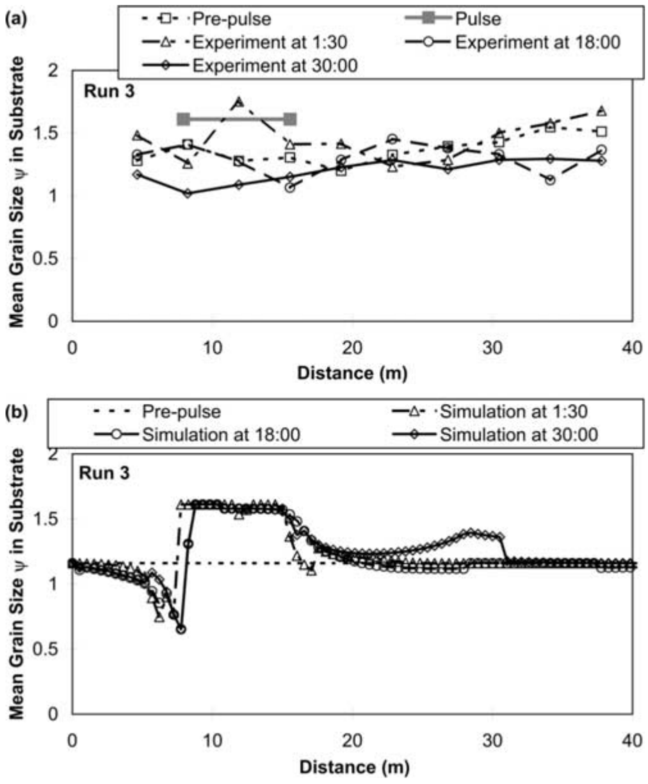

Figure 7. (a) Observed temporal and spatial variation in substrate mean grain size on the psi scale for run 3. The times are in (hour:min). The line for the time 0:00, i.e., the initial condition, characterizes the bed before the placement of the pulse. (b) Simulated temporal and spatial variation in substrate mean grain size on the psi scale for run 3. The times are in (hour:min). The line for the time 0:00, i.e., the initial condition, characterizes the bed before the placement of the pulse.

from points of very low predicted deviation from the ambient elevation (i.e., a bed elevation that deviates from equilibrium elevation by less than 10^{-5} m). In the initial stages of pulse deformation, i.e., up to the first 9 min the model did an excellent job of describing pulse evolution, which was almost entirely dispersive. After that time, however, the observed pulse began to show significant translation as well as dispersion. The numerical model also showed translation, but the onset of the phenomenon was delayed by about 20 min as compared to the measurements.

[31] Figure 10b shows an interesting prediction of the model. At times 1:00 and 2:00 some scour is predicted below the ambient bed in a zone corresponding to the upstream end of the initial position of the pulse. This scour is predicted because the mixing of sand into the initially coarser ambient bed renders the effective surface size smaller, and the sediment more mobile than under ambient conditions. The resolution of Figure 10a does not allow for the confirmation of this phenomenon in the experimental data.

[32] Run 4b progressed so quickly that it was not possible to measure the time variation in surface and substrate grain size distributions. Figures 11a–11c, however, illustrate the predicted and observed patterns of sediment transport rate (Figure 11a), percentage of sand in the load (Figure 11b)

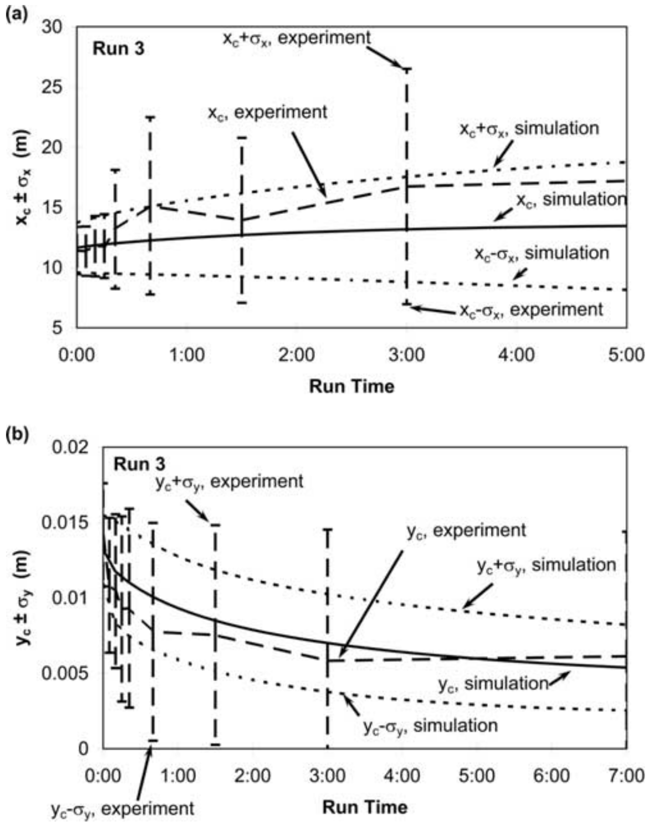

Figure 8. (a) Simulated and observed temporal variation in x_c and $x_c \pm \sigma_x$ for run 3. The vertical lines show the experimental spread from $x_c - \sigma_x$ to $x_c + \sigma_x$. (b) Simulated and observed temporal variation in y_c and $y_c \pm \sigma_y$ for run 3. The vertical lines show the experimental spread from $y_c - \sigma_y$ to $y_c + \sigma_y$.

and bed load arithmetic mean grain size Ψ_m on the Ψ scale (Figure 11c). The simulated patterns have broadly the same forms as the observed patterns, but are significantly delayed in time compared to the observations. In addition, the model did not predict the rapid recovery of bed load arithmetic grain size after the pulse passed through that is evident in Figure 11c for the experimental results. This again underlines the slower translation predicted by the model; the recovery would have been evident had the numerical run been continued beyond the time of the experimental run. In Figures 11b and 11c, the simulated bed load first becomes slightly coarser as the pulse sediment arrives at a station,

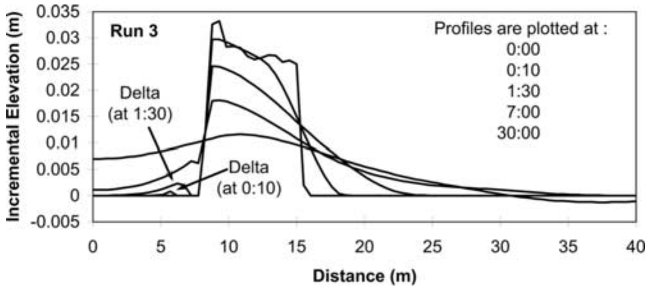

Figure 9. Plot of simulated incremental bed elevations for run 3. The times are in (hour:min).

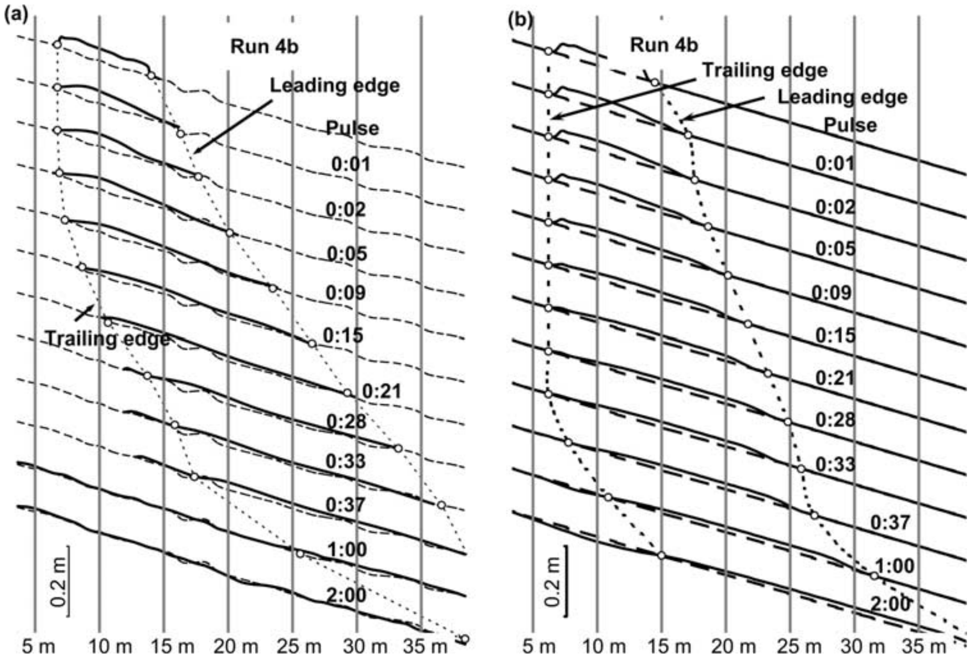

Figure 10. (a) Observed long profiles of cross-sectionally averaged bed elevation for run 4b. The times are in (hour:min). (b) Simulated long profiles of bed elevation for run 4b. The times are in (hour:min).

and then quickly becomes substantially finer. The initial slight coarsening is a result of the sand reducing the geometric mean size of the surface layer, thus increasing gravel mobility. With arrival of increasing quantities of sand, however, the bed load quickly becomes much finer. The experimental data are not of sufficient accuracy to resolve any initial coarsening of the bed before it becomes swamped by sand.

[33] It can be seen from Figure 12a that the prediction for x_c is low, mostly because of the significant translation of the pulse observed experimentally between about 10 and 30 min after the run was commenced. Figure 12b demonstrates that the model provided an accurate representation of the process of thinning of the pulse as it deformed, as measured in terms of decreasing y_c.

5. Discussion

[34] As noted previously in this paper, the experiments are not ideal for testing the numerical model because of the relatively fine grain sizes and abundance of sand. It should be noted, however, that the coarse pulse of run 3 was specifically designed to provide the best possible test of the model. As might be expected, the performance of the model proved good in this case. In particular, the ability of the model to reproduce the delta observed upstream of the pulse (but not necessarily the details of its shape) is notable.

[35] In the case of all three runs the numerical model successfully predicted the dominance of dispersion over translation. In the case of run 2, the model under-predicted the rate of deformation of the pulse. This is partially due to an under-prediction of sediment transport by the model. The model could probably be adjusted to provide better agreement, but this would defeat the purpose of the test, which is to provide insight into the behavior of sediment pulses in rivers.

[36] The worst performance of the model might be expected in the case of run 4b, for which the pulse consisted entirely of sand. The model, however, provided a remarkably good prediction of pulse deformation for the first 9 min. This initial period was characterized essentially by dispersion. It also provided a reasonably accurate prediction of the time variation of the average thickness of the pulse, as measured in terms of y_c, for the duration of the run. After the first 9 min the experimental pulse began to translate downstream. The model did not reproduce this feature until 20 min later.

[37] The sediment transport model used here has also been used to predict the formation of translating sheets of finer gravel of minimal topographic expression moving over coarser gravel [*Seminara et al.*, 1996]. These gravel sheets have been studied experimentally, e.g., by *Whiting et al.* [1988]. Thus it should come as no surprise that the model reproduces the observed tendency of the sand pulse to devolve into a translating sheet upon becoming sufficiently thin. *Lisle et al.* [1997] report that thinning of a pulse promotes translation. There could, however, be several reasons why the onset of translation was significantly delayed in the model. The most obvious of them might be the expected inability of the model to predict sand transport accurately.

6. Numerical Runs for a Sand Bed River at Low Slope

[38] As noted above, experimental pulses were observed to be predominantly dispersive, a result also predicted by the numerical model. There are two reasons for this; the high Froude number *Fr* of the ambient flow and the fact that the initial pulses had lengths that were much larger than the ambient depth [*Lisle et al.*, 1997, *Cui and Parker*, 1997b]. As the Froude number becomes lower and the pulse length

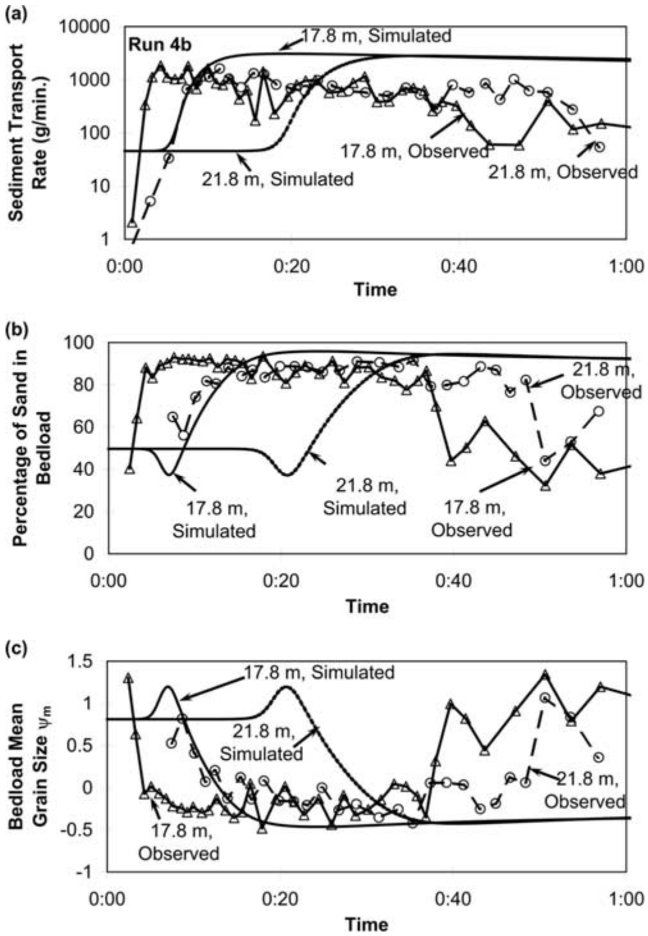

Figure 11. (a) Simulated and observed temporal variation in sediment transport rate at two sites in run 4b. (b) Simulated and observed temporal variation in the fraction of sand in transport at two sites in run 4b. (c) Simulated and observed temporal variation in arithmetic mean bed load size Ψ_m at two sites in run 4b.

becomes shorter translation becomes relatively more important. For this reason significant pulse translation (in addition to dispersion) might be expected in low-slope sand bed streams.

[39] In order to test this idea, the model was adapted to such streams. The *Brownlie* [1981] relations for sediment transport and flow resistance were used for this purpose in place of those of *Parker* [1990a, 1990b] and (9), respectively. The sediment was assumed to be sand with a median size D_{50} of 0.2 mm and a geometric standard deviation σ_g of 1.5. The ambient equilibrium flow had a water discharge per unit width q_w of 10 m^2/s, a bed slope S of 1×10^{-4}, a depth h of 5.07 m, a flow velocity u of 1.97 m/s and a Froude number *Fr* of 0.28, i.e., well into the subcritical range. These numbers are loosely based on the Fly River upstream of D'Albertis Junction, Papua New Guinea [*Dietrich et al.*, 1999]. The initial pulse is taken to be a parabola 2 km long and 1 m high composed of the same sand as the ambient bed material. The predicted deformation of this pulse shows significant translation as well as dispersion, as evidenced in Figure 13.

[40] It should be noted that the *Brownlie* [1981] relation is designed for sand bed streams, and does not calculate sediment transport on a grain size specific basis. As a result it is not suitable for use in comparison with the experimental results of part 1.

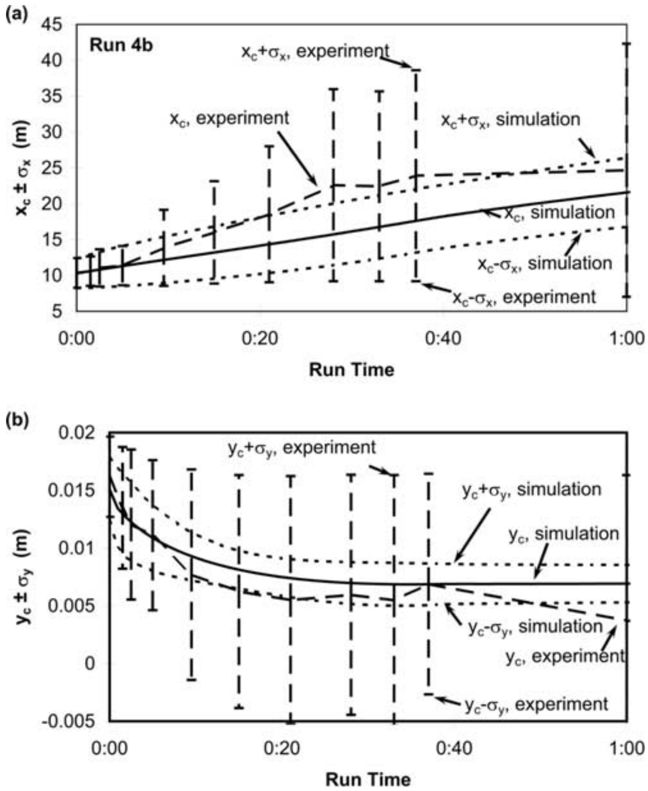

Figure 12. (a) Simulated and observed temporal variation in x_c and $x_c \pm \sigma_x$ for run 4b. The vertical lines show the experimental spread from $x_c - \sigma_x$ to $x_c + \sigma_x$. (b) Simulated and observed temporal variation in y_c and $y_c \pm \sigma_y$ for run 4b. The vertical lines show the experimental spread from $y_c - \sigma_y$ to $y_c + \sigma_y$.

7. Conclusions

[41] A numerical model designed for the simulation of sediment pulses in mountain rivers at field scale was tested against the experimental pulses of part 1, the companion to

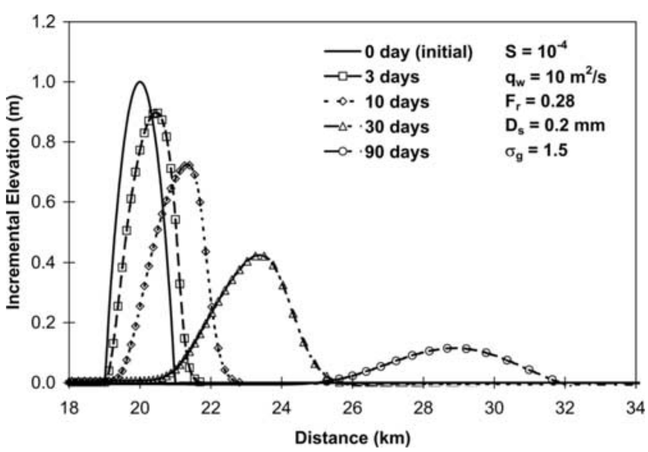

Figure 13. Simulated deformation of sediment pulse in a low-slope sand bed stream.

this paper. The comparison was not expected to be perfect because the sediment in the experiments is considerably finer than the gravel for which the model is designed. This notwithstanding, the model successfully reproduced the predominantly dispersive deformation of the experimental pulses.

[42] The model performed best when the pulse was significantly coarser than the ambient sediment, achieving reasonable agreement with the data in most parameters. Of interest in this case was the ability of the model to predict the formation of a delta in the backwater zone of the pulse. This delta was also observed in the experiment. The reasonable agreement when compared against the results for the coarsest pulse lends some credence to the applicability of the model to field-scale mountain gravel bed rivers, where it has already been shown to perform well in the case of the Navarro River [*Sutherland et al.*, 1998; *Hansler et al.*, 1998; *Sutherland et al.*, 2002]. This is not meant to imply that the model can be applied in the field only to cases for which the pulse is significantly coarser than the ambient load. Rather, it implies that the experiment using the coarsest sediment best models gravel transport in the field, and thus is closest to the conditions under which the sediment transport model might be expected to work. It should be noted that gravel dominates in the grain size distributions of the Navarro River, placing it at the center of expected applicability of the bed load transport relation of *Parker* [1990a, 1990b].

[43] The model performance generally became poorer as finer pulse sediment was considered, with the least acceptable performance for the case of run 4b. This notwithstanding, the model was able to predict both dispersion and translation of the finest pulse. Both these features were observed in the experiment. The model under-predicted the degree of translation. Both the model and the experiments suggest that translation becomes increasingly important as the pulse sediment becomes fine and as the pulse disperses to a thin sheet. Such thin translational pulses likely constitute members of the class of gravel sheets [e.g., *Whiting et al.*, 1988].

[44] The reason for the predominance of dispersion in these experiments is the high Froude number of the ambient flow, a feature also to be expected in mountain gravel bed streams in flood. Additional factors promoting dispersion are an initial pulse length that is long compared to ambient depth and a pulse height greater than the flow depth. When the model is adapted to conditions characteristic of large, low-slope sand bed streams with low Froude numbers it predicts substantial translation as well as dispersion.

Notation

- dA elemental unit of area in the x-y plane.
- D grain size, mm.
- D_{f50} median size of sediment feed material.
- D_j lower bound the jth grain size range.
- $\overline{D}_j$ mean size of the jth grain size range.
- D_{50} median grain size.
- D_{p50} median size of sediment in the initial pulse.
- D_{sg} surface geometric mean grain size.
- D_{sub} substrate geometric mean grain size.
- D_{sur} surface geometric mean grain size.
- F_j mass fraction of sediment in the surface layer in the jth grain size range.
- $f_{I,j}$ mass fraction of sediment in the jth grain size range of sediment exchanged at the surface-substrate interface as the bed aggrades or degrades.
- Fr Froude number of flow.
- g gravitational acceleration.
- h flow depth.
- k_s roughness height.
- L_a thickness of surface (active, exchange) layer of sediment.
- p_j mass fraction of the bed load in the jth grain size range.
- $p_{S,j}$ mass fraction of the substrate immediately below the active layer in the jth grain size range.
- q_G volume gravel transport rate per unit width.
- q_w water discharge per unit width.
- S bed slope.
- t time.
- u flow velocity.
- u_* shear velocity.
- x down-channel distance.
- x_c down-channel coordinate of the centroid of a pulse.
- y distance measured upward from the ambient bed.
- y_c upward coordinate of the centroid of a pulse.
- α coefficient relating k_s and L_a in equation (10).
- χ coefficient in equation (8).
- ϕ grain size on the phi scale; $= -\log_2(D)$.
- η bed elevation.
- λ_p bed porosity.
- σ_g geometric standard deviation of the size distribution.
- σ_{sg} geometric standard deviation of the surface size distribution.
- σ_x down-channel component of the standard deviation of pulse shape about its centroid.
- σ_y upward component of the standard deviation of pulse shape about its centroid.
- τ^*_{rsgo} reference Shields stress in the *Parker* [1990a, 1990b] bed load relation.
- ψ grain size on the psi scale; $= \log_2(D)$.
- ψ_j lower bound on the psi scale of the jth grain size range.
- $\overline{\Psi}_j$ characteristic size on the psi scale of the jth size range.
- ψ_m arithmetic mean grain size on the psi scale.

[46] **Acknowledgments.** This research was funded jointly by the U.S. Environmental Protection Agency and the U.S. National Science Foundation (EPA/R824779-01-0 and NSF/EAR-9524358). Resources supplied by the Minnesota Supercomputer Institute are gratefully acknowledged. The support of the first author's current employer, Stillwater Sciences, is gratefully acknowledged. The extensive, helpful suggestions of P. Ashmore, S. Coleman, A. P. Nicholas, and two anonymous reviewers have been incorporated into the text.

References

Benda, L., and T. Dunne, Stochastic forcing of sediment routing and storage in channel networks, *Water Resour. Res.*, *33*(12), 2865–2880, 1997.

Brownlie, W. R., Prediction of flow depth and sediment discharge in open channels, *Rep. KH-R-43A*, 232 pp., W.M. Keck Lab. of Hydraul. and Water Resour., Calif. Inst. of Technol., Pasadena, 1981.

Cui, Y., and G. Parker, A quasi-normal simulation of aggradation and downstream fining with shock fitting, *Int. J. Sediment. Res.*, *12*(2), 68–82, 1997a.

Cui, Y., and G. Parker, Linear analysis of coupled equations for sediment transport, paper presented at Theme B, 27th Congress, Int. Assoc. of Hydraul. Res., San Francisco, Calif., 1997b.

Cui, Y., and G. Parker, Numerical model of sediment pulses and sediment supply disturbances in mountain rivers, *J. Hydraul. Eng.*, in press, 2003.

Cui, Y., G. Parker, and C. Paola, Numerical simulation of aggradation and downstream fining, *J. Hyrdaul. Res.*, *32*(2), 185–204, 1996.

Cui, Y., G. Parker, T. E. Lisle, J. Gott, M. E. Hansler-Ball, J. E. Pizzuto, N. E. Allmendinger, and J. M. Reed, Sediment pulses in mountain rivers: 1. Experiments, *Water Resour. Res.*, *39*, doi:10.1029/2002WR001803, in press, 2003.

Dietrich, W. D., G. Day, and G. Parker, The Fly River, Papua New Guinea: Inferences about river dynamics, floodplain sedimentation and fate of sediment, in *Varieties of Fluvial Form*, edited by A. J. Miller and A. Gupta, pp. 345–376, John Wiley, Hoboken, N. J., 1999.

Hansler, M. E., D. G. Sutherland, S. J. Hilton, and T. E. Lisle, Sediment wave dispersion and the analysis of a one-dimensional bedload transport model, Navarro River, California, *Geol. Soc. Am. Abstr. Programs*, *29*(6), A–360, 1998.

Li, T. L., R. L. Schuster, and J. Wu, Landslide dams in south-central China, in *Landslide Dams: Processes, Risk and Mitigation*, *Geotech. Spec. Publ.*, vol. 3, edited by R. L. Schuster, Am. Soc. of Civ. Eng., Reston, Va., 1986.

Lisle, T. E., J. E. Pizzuto, H. Ikeda, F. Iseya, and Y. Kodama, Evolution of a sediment wave in an experimental channel, *Water Resour. Res.*, *33*(8), 1971–1981, 1997.

Lisle, T. E., Y. Cui, G. Parker, J. E. Pizzuto, and A. M. Dodd, The dominance of dispersion in the evolution of bed material waves in gravel-bed rivers, *Earth Surf. Processes Landforms*, *26*, 1409–1422, 2001.

Parker, G., Surface-based bedload transport relation for gravel rivers, *J. Hydraul. Res.*, *28*(4), 417–436, 1990a.

Parker, G., The ACRONYM series of PASCAL programs for computing bedload transport in gravel rivers, *External Memo. M-220*, 124 pp., St. Anthony Falls Lab., Univ. of Minn., Minneapolis, 1990b.

Parker, G., Selective sorting and abrasion of river gravel. I: Theory, *J. Hydraul. Eng.*, *117*(2), 131–149, 1991a.

Parker, G., Selective sorting and abrasion of river gravel. II: Application, *J. Hydraul. Eng.*, *117*(2), 150–171, 1991b.

Seminara, G., M. Colombini, and G. Parker, Nearly pure sorting waves and formation of bedload sheets, *J. Fluid Mech.*, *312*, 253–278, 1996.

Sutherland, D. G., M. E. Hansler, S. J. Hilton, and T. E. Lisle, Sediment wave evolution and channel morphologic changes resulting from a landslide, Navarro River, northwestern California, *Geol. Soc. Am. Abstr. Programs*, *29*(6), A–360, 1998.

Sutherland, D. G., M. Hansler-Ball, S. J. Hilton, and T. E. Lisle, Evolution of a landslide-induced sediment wave in the Navarro River, California, *Geol. Soc. Am. Bull.*, *114*(8), 1036–1048, 2002.

Toro-Escobar, C. M., G. Parker, and C. Paola, Transfer function for the deposition of poorly sorted gravel in response to streambed aggradation, *J. Hydraul. Res.*, *34*(1), 35–53, 1996.

Whiting, P. J., W. E. Dietrich, L. B. Leopold, T. G. Drake, and R. L. Shreve, Bedload sheets in heterogeneous sediment, *Geology*, *16*, 105–109, 1988.

Wilcock, P. R., and J. C. Crowe, A surface-based transport model for sand and gravel, *J. Hydraul. Eng.*, *129*(2), 120–128, 2003.

Y. Cui, Stillwater Sciences, 2532 Durant Avenue, Berkeley, CA 94704, USA. (yantao@stillwatersci.com)

T. E. Lisle, Pacific Southwest Research Station, Forest Service, U.S. Department of Agriculture, 1700 Bayview Drive, Arcata, CA 95521, USA.

G. Parker, St. Anthony Falls Laboratory, University of Minnesota, Mississippi River at Third Avenue, S.E., Minneapolis, MN 55414, USA. (parke002@umn.edu)

J. E. Pizzuto, Department of Geology, University of Delaware, Newark, DE 19716, USA.